

Potential Exploration of Recent FDA-Approved Anticancer Drugs Against Models of SARS-CoV-2's Main Protease and Spike Glycoprotein: A Computational Study

Shazia Parveen^{1,*} , Rua B Alnoman¹ 

¹ Faculty of Science, Chemistry Department, Taibah University, Yanbu Branch, 46423, Yanbu, Saudi Arabia

* Correspondence: shazia021@gmail.com

Scopus Author ID 57187913400

Received: 20.09.2020; Revised: 9.10.2020; Accepted: 10.10.2020; Published: 12.10.2020

Abstract: COVID-19 has become a worldwide risk to the healthcare system of practically every nation of the world, which originated from Wuhan, China. To date, no specific drugs are available to treat this disease. The exact source of the SARS-CoV-2 is yet unknown, although the early cases are associated with the Seafood market in Huanan, South China. This manuscript reports the *in silico* molecular modeling of recent FDA-approved anticancer drugs (Capmatinib, Pemigatinib, Selpercatinib, and Tucatinib) for their inhibitory action against COVID-19 targets. The selected anticancer drugs are docked on SARS-CoV-2 main protease (PDB ID: 6LU7) and SARS-CoV-2 spike glycoprotein (PDB ID: 6M0J) to ascertain the binding ability of these drugs. ADMET parameters of the drugs are assessed, and in addition, DFT calculations are done to investigate the pharmacokinetics, thermal parameters, dipole moments, and chemical reactivity descriptors. The docking energies (ΔG) and the interacting amino acid residues are discussed. Promising molecular docking conclusions have been accomplished, which demonstrated the potential of selected anticancer drugs for plausible drug development to fight COVID-19. Further optimizations with the drug may support the much-needed rapid response to mitigate the pandemic.

Keywords: Artemisinins; VEGFR-2; ADME; molecular docking; DFT.

Abbreviations: ADME-Absorption, distribution, metabolism, and excretion; ARDS-Acute respiratory distress syndrome; CoV-Coronavirus; COVID-19-Coronavirus Disease 2019; DFT-Density functional theory; FDA-Food and drug administration; FMO-Frontier molecular orbital; HER2-Human epidermal growth factor receptor 2; HOMO-Highest occupied molecular orbital; LUMO-Lowest unoccupied molecular orbital; MW-Molecular weight; PDB-Protein data bank; RdRp-RNA-dependent RNA polymerase; RNA-Ribonucleic acid; SARS-CoV-2-Severe acute respiratory syndrome coronavirus 2; WHO-World health organization.

© 2020 by the authors. This article is an open-access article distributed under the terms and conditions of the Creative Commons Attribution (CC BY) license (<https://creativecommons.org/licenses/by/4.0/>).

1. Introduction

Worldwide, as of 30 September 2020, there have been 33,441,919 confirmed cases of COVID-19, including 1,003,497 deaths, reported to WHO (<https://covid19.who.int/>). As per a published report on ProMED-mail in December 2019, a group of patients was found to exhibit pneumonia-like symptoms of unknown etiology in Wuhan city, Hubei Province, China (<https://promedmail.org/>). Later on February 12, 2020, the novel coronavirus was found responsible for the cause, was officially named as 2019 novel coronavirus (2019-

nCoV)/Coronavirus Disease 2019 (COVID-19) by WHO. And WHO declared COVID-19 outbreak a pandemic on 11 March [1].

Human coronaviruses are positive-sense, 30,000 bp long, single-stranded RNA viruses that belong to the *Coronaviridae* family, responsible for various diseases with enteric, respiratory, hepatic, and neurological symptoms [2]. SARS-CoV-2 was responsible for infection in pets and respiratory diseases of variable severity in humans (*i.e.*, severe acute respiratory syndrome coronavirus 2, abbreviated as SARS-CoV-2). Therefore, human infecting coronavirus can be classified into low and highly pathogenic [3]. SARS-CoV-2 is possibly a new recombinant β -coronavirus that originated from bats. The recombination occurred within the Spike glycoprotein, which recognizes a cell surface receptor, consequently permitting transmission amid different species [4]. Two classes of proteins that typify coronaviruses are structural proteins (*viz.*, spike, nucleocapsid, matrix, and envelope) and nonstructural proteins (*viz.*, proteases and RdRp; RNA-dependent RNA polymerase) [5]. Spike protein in a homotrimeric state is present on the outer surface of the virus; it is a vital recognition factor for the attachment and entry of the virus into the host cells [6,7]. Currently, there has been an exponential increase in the number of established infections; nonetheless, there is no definite treatment for symptoms caused in COVID-19. The severity of COVID-19 requires an urgency to develop a vaccine within the record-breaking time of ~12-18 months.

The methodology involved in the development of a new drug, preclinical research, and its approval is costly and almost a decade long process. This time-taking discovery procedure unravels the scope of drug repurposing as an alternate methodology for reducing the time required for drug development [8]. These days, the idea of drug repurposing is comprehensively used for the identification of previously approved (or under investigation or even discarded drugs) for several other diseases, because of the fact that various drugs might be able to target multiple proteins and not just one, and also many diseases constitute an overlapping molecular pathway. Despite the fact that the drug repurposing approach is old, it has earned considerable stimulus in the past 10 years: about 1/3rd of the drug approvals in current years is owed to drug repurposing, producing ~25% of the annual revenue for the pharma industry [9,10].

COVID-19 is a mild-to-severe respiratory illness linked with symptoms causing fever, fatigue, dry cough, muscle aches, shortness of breath, pneumonia [11,12]. Its severity might lead to ARDS (Acute respiratory distress syndrome), which is characterized by inflammation in the lungs with fluid build-up within the lungs and its vicinity that causes septic shock because of intense fall in the blood pressure causing a shortage of oxygen to the body organs. The incubation period of COVID-19 is ~1 to 14 days [13]. In particular, a remarkable number of drugs reconsidered for treatment of COVID-19 either are or have been used in treating cancer [14]. Virus-infected human cells are compelled to boost up the synthesis of nucleic acids, proteins, and lipids, enhancing energy metabolism so as to confirm the “viral program”. Undeniably, cancer cells also display similar features, suggesting that drugs used to treat cancer, which interferes with specific cancer cell pathways, could be effective against viral replication. To our awareness, cancer therapeutic drugs that could have the potential for treating COVID-19 have not been comprehensively studied.

Therefore, in search of a coherent and effective choice of drugs suitable for repurposing for the treatment of SARS-CoV-2 [15,16]. We here in this paper, report the *in silico* evaluation of recent FDA-approved anticancer drugs against two very important SARS-CoV-2 targets *viz.*, main protease [17–22] and spike glycoprotein [23–25]. We have chosen four recently approved

anticancer drugs- Capmatinib* that got approval under trade name Tabrecta FDA in June 2020 for treating non-small cell lung cancer; Pemigatinib[†] (Pemazyre) approved in April 2020 cholangiocarcinoma, a rare form of bile duct cancer; Selpercatinib[‡] (Retevmo) for the treatment of lung and thyroid cancers got approval in May 2020. Tucatinib^{§§} (Tukysa) to treat advanced unresectable or metastatic HER2-positive breast cancer approved in April 2020. SARS-CoV-2 main protease is known to be accountable for monitoring numerous key viral functions that include viral replication processes making it an ideal target for drug development [26]. The second *in silico* docking model is the spike protein, which is a key recognition factor responsible for virus attachment and entry into the host cells. Therefore, we studied the synergistic effect of the selected drugs against the SARS-CoV-2 main protease (PDB ID: 6LU7) and SARS-CoV-2 spike glycoprotein (PDB ID: 6M0J) *via* molecular docking and DFT calculations. The results are promising and suggest possible inhibition for the currently available cancer therapeutics against the newly emerged COVID-19.

2. Materials and Methods

2.1. *In silico* ADME and drug-likeness.

Physically substantial descriptors and pharmaceutically significant properties of all the selected drugs *viz.*, MW, mlogP, H-bond donors, and H-bond acceptors in accordance with the Lipinski's rule of five were explored. The ADMET parameters of the selected anticancer drugs were also predicted using SwissADME (<http://www.swissadme.ch/index.php>) [27]. *In silico* analyses to guess the core pharmacokinetics parameters such as blood-brain barrier (BBB) permeability, gastrointestinal (GI) absorption, P-glycoprotein-mediated efflux (Pgp) were also carried out.

2.2. DFT calculations.

DFT has been proved to be a powerful tool for the study of electronic and thermodynamic parameters. The quantum computational studies of anticancer drugs were performed in the gas phase on GAMESS [28,29]. Considering the complexity of the theoretical model used for this study, all the structural optimizations were carried out at the DFT using a basis set of B3LYP/6-31G(d) method. The electronic properties of the drugs such as E_{HOMO} , E_{LUMO} , HOMO-LUMO energy gap, global hardness, electronegativity, electronic chemical potential, electrophilicity, and chemical softness, natural charges, and dipole moment were calculated [30–32].

2.3. Molecular docking.

Docking calculations were done on AutoDock Vina [33]. Energy minimized structure of anticancer drugs Capmatinib, Pemigatinib, Selpercatinib, and Tucatinib, obtained from DFT optimization, were utilized for docking analyses. The crystal structures of SARS CoV-2 main protease (PDB ID: 6LU7) [34] and SARS-CoV-2 spike glycoprotein (PDB ID: 6M0J) [35] were retrieved from the Protein Data Bank (<http://www.rcsb.org/pdb>) in PDB format and were prepared by AutoDock Tools [36]. A grid box of $40 \times 40 \times 40$ Å centered at (-25.986, 12.590, 59.154) Å and (-26.858, 18.390, -13.832) Å, for the SARS-CoV-2 main protease and SARS-CoV-2 spike glycoprotein, respectively, was used in the docking experiments. Visualization of

the docked poses has been done by CHIMERA (www.cgl.ucsf.edu/chimera) [37] and Discovery Studio visualizer [38].

3. Results and Discussion

3.1. *In silico* ADME and drug-likeness.

The major parameters for pharmacokinetics are ADME (absorption, distribution, metabolism, and excretion) [39]. Table 1 shows predicted *in silico* ADME properties of selected anticancer drugs. The results were suggestive of no significant violations of the Lipinski's rule of five [40], as all calculated values fall within the expected range. As per this model, the drugs displayed acceptable bioavailability orally along with other parameters *viz.*, lipophilicity, MW, polarity, solubility, saturation, flexibility as exposed in bioavailability radar plots [41].

Table 1. Selected calculated physicochemical and pharmacokinetic properties of investigated drugs.

Properties	Capmatinib	Pemigatinib	Selpercatinib	Tucatinib
mLogP	2.80	2.34	1.35	3.19
TPSA (Å ²)	85.07	83.16	112.04	110.85
MW (g/mol)	412.42	487.50	525.60	480.52
nHBA	6	8	8	7
nHBD	1	1	1	2
n violations	0	0	1	0
Nrotb	5	6	8	6
GI absorption	High	High	High	High
BBB permeant	No	No	No	No
Pgp substrate	Yes	Yes	Yes	Yes
LogS	-4.39	-3.19	-4.50	-6.02

mLogP= lipophilicity; TPSA= Total Polar Surface Area; MW= Molecular Weight; nHBA= number of hydrogen bond acceptors; nHBD= number of hydrogen bond donors; n violations= number of violated drug-likeness rules; nrotb= number of rotating bonds; BBB= blood-brain barrier; GI= gastrointestinal; Pgp= p-glycoprotein; LogS= solubility.

Lipophilicity is described by the partition coefficient between n-octanol and water (log Po/w or mlogP), a significant parameter for pharmacokinetics drug discovery ascertained by SwissADME [42,43]. mlogP values for all four investigated drugs were below 4.15, especially low in the case of Selpercatinib due to increased electron density and polarity since Selpercatinib exhibit the highest dipole moment value ascertained by DFT calculations later. On the other hand, Tucatinib has the highest lipophilicity owing to the presence of fluorine that boosts its lipid solubility. However, the positive mlogP values imply that all the investigated anticancer drugs have sufficient lipophilicity and accomplish the critical criteria for drug moiety. Water solubility is another significant prerequisite for any drug moiety that is expected to be administered orally given in an adequate quantity of the active pharmaceutical ingredients in a small amount [44,45]. From the values of LogS, we can conclude that Pemigatinib exhibited good water solubility while the other three were found to be moderately soluble, displaying predicted solubility ranging between -4 to -6. These findings suggested that the selected drugs were capable of oral administration in the body.

The number of free rotatable bonds and Lipinski's rule determined the drug-likeness. *In silico* studies were carried out to predict the core pharmacokinetic parameters such as gastrointestinal absorption, P-glycoprotein-mediated efflux (Table 1). All these investigated anticancer drugs Capmatinib, Pemigatinib, Selpercatinib, and Tucatinib, display high gastrointestinal absorption, which permits their oral dosing.

Bioavailability radar of anticancer drugs Capmatinib, Pemigatinib, Selpercatinib, and Tucatinib ascertained from SwissADME showed that they exhibit excellent predicted physicochemical descriptors and pharmacokinetic properties for oral bioavailability (Figure 1). The perfect space of six physicochemical parameters for oral bioavailability- size, polarity, lipophilicity, solubility, flexibility, and saturation are located within the pink-colored area [41,46]. All four investigated anticancer drugs are present in the pink area, i.e., agreeable area, except in Capmatinib and Tucatinib, the fraction of sp^3 hybridized carbons is <0.25 [41].

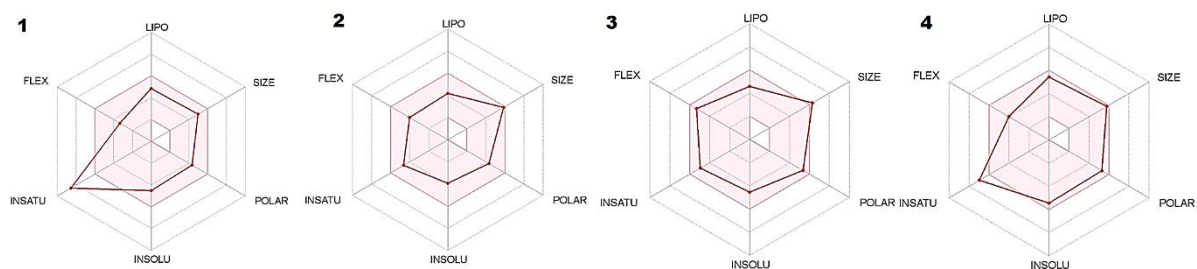


Figure 1. Bioavailability radar plot of investigated anticancer drugs; Capmatinib (1), Pemigatinib (2), Selpercatinib (3), and Tucatinib (4). POLAR (polarity), LIPO (lipophilicity), INSOLU (solubility), FLEX (flexibility), and INSATU (saturation).

3.2. DFT calculations.

DFT, a computer-based method that has gained a vast status in the area of *in silico* pharmaceutical analysis, was implemented to evaluate the electronic and reactivity parameters of the investigated anticancer drugs. The study of the electronic parameters of the molecules plays a vital role in determining the pharmacological properties. DFT optimized structures of selected anticancer drugs are shown in Figure 2. Frontier molecular orbitals (FMOs) are- i) HOMO (highest occupied molecular orbital), the highest energy orbital occupied with electrons, hence an electron donor, and ii) LUMO (lowest unoccupied molecular orbital), the lowest energy orbital that can accept electrons, hence an electron acceptor. These FMOs control the mode of the interaction of the drugs with other molecules. Furthermore, these drugs were investigated on the basis of HOMO/LUMO energy gaps.

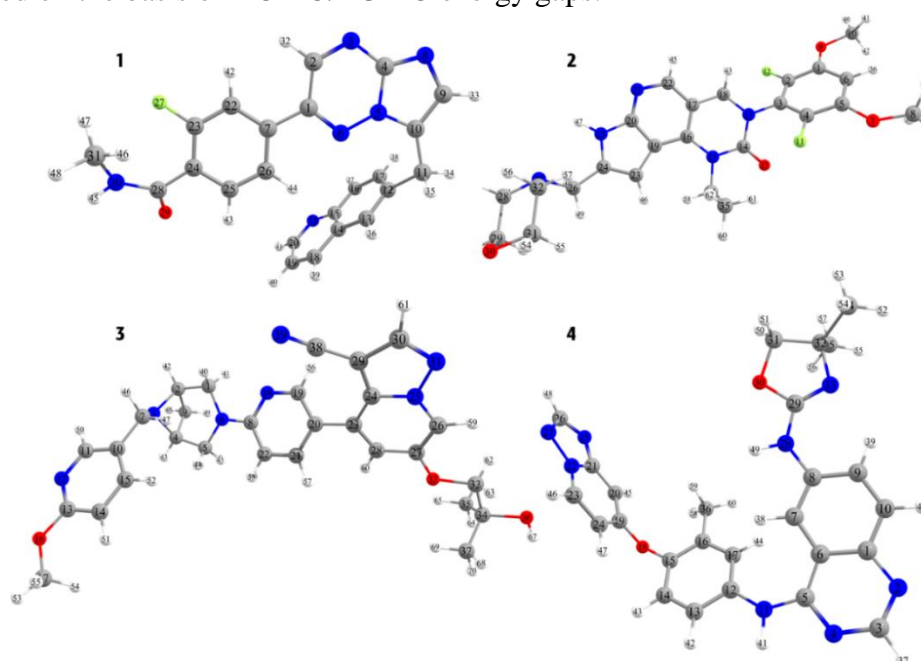


Figure 2. DFT-optimized geometries of Capmatinib (1), Pemigatinib (2), Selpercatinib (3), and Tucatinib (4).

As a general rule, the increase in the energy gap leads to decreased reactivity and vice versa [47]. B3LYP functional method was applied for DFT calculations, while for calculating the band energy gap, (ΔE) expression of $E_{LUMO}-E_{HOMO}$ was used [48]. The results are summarized in Table 2.

Table 2. Thermal parameters (Hartree/Particle) (KJ/mol) and Dipole moment (Debye) of investigated drugs.

Parameters	Capmatinib	Pemigatinib	Selpercatinib	Tucatinib
ZPVE	1022.676	1394.367	1591.966	1323.790
E_{tot}	1077.157	1464.903	1668.228	1389.819
H	1079.636	1467.382	1670.706	1392.298
G	895.236	1251.460	1440.592	1184.248
μ	5.291	3.066	9.605	2.299

ZPVE: Sum of electronic and zero-point energies; E_{tot} : Sum of electronic and thermal energies; H: Sum of electronic and thermal enthalpies; G: Free energy; μ : Total Dipole Moment.

In addition to HOMO and LUMO, some other chemical reactivity descriptors *viz.*, chemical hardness (η), chemical softness (σ), electrophilicity index (ω), nucleophilic index (ϵ), electronegativity (χ), and chemical potential (μ) were also calculated and are summarized in Table 3 [30–32]. All these parameters, combined with different extents, exert a significant impact on the degree of the binding affinity of drugs with active drug targets.

Table 3. The theoretical calculated conceptual DFT descriptors of investigated drugs.

Parameters	Capmatinib	Pemigatinib	Selpercatinib	Tucatinib
E_{HOMO} (a.u.)	-0.313	-0.282	-0.278	-0.282
E_{LUMO} (a.u.)	0.031	0.108	0.068	0.067
$E_g(HOMO-LUMO)$ (a.u.)	-0.344	-0.390	-0.346	-0.349
$\Delta E(LUMO-HOMO)$	0.344	0.390	0.346	0.349
Electronegativity (χ)	0.141	0.087	0.105	0.107
Chemical hardness (η)	0.172	0.195	0.173	0.174
Chemical softness (σ)	7.0921	11.4942	9.5238	9.3023
Chemical potential (μ)	-0.141	-0.087	-0.105	-0.107
Electrophilicity index (ω)	-0.0575	-0.0193	-0.0317	-0.0329
Nucleophilic index (ϵ)	-0.0242	-0.0169	-0.0181	-0.0187

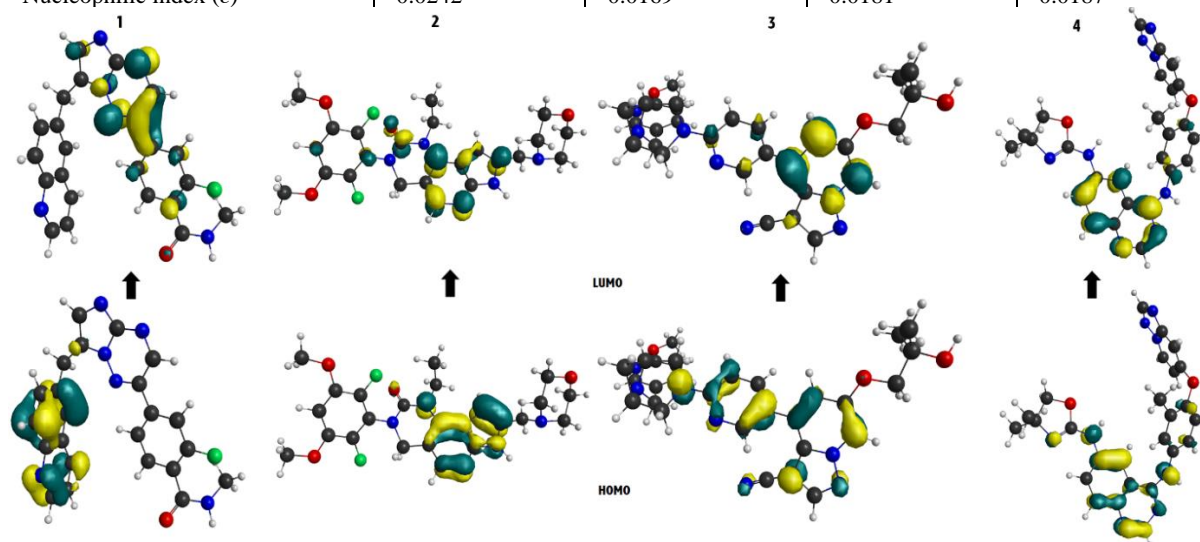


Figure 3. HOMO-LUMO energy of optimized structures of Capmatinib (1), Pemigatinib (2), Selpercatinib (3), and Tucatinib (4).

Figure 3 shows the three-dimensional plots of FMOs (HOMO and LUMO) in the optimized state. In addition, the thermodynamic parameters were also calculated and are summarized in Table 3. The dipole moment is a significant electronic property and was found to be in the order Selpercatinib (9.605 Debye) > Capmatinib (5.291 Debye) > Pemigatinib

(3.066 Debye) > Tucatinib (2.299 Debye). A large dipole moment represents very strong intermolecular interactions [49].

3.3. Molecular docking.

Molecular docking is an *in silico* method that analyzes the binding properties of the ligands [50–52]. The ligand binding in the active site of the selected target is suggestive of the possibility that the ligand may probably be able to steer functional modification of the target molecules [53,54]. The drug-target interactions were also deciphered in terms of the amino acid residues, interacted with the drug, the hydrogen bonding, analysis of the molecular docking energy (ΔG , kcal/mol), and comparing the amino acid residues in the active sites and feasible binding sites.

3.3.1. Docking with SARS-CoV-2 main protease.

SARS-CoV-2 main protease is a homo-dimeric protein with two subunits; each having a length of 306 residues and contain 9 α -helices and 13 β -strands to form 3 discrete domains: I (from residues 8 to 100), II (from residues 101 to 184), and III (from residues 199 to 306) (Figure 4A) [34]. Domain III comprises of 5 α -helices ($\alpha 5$ - $\alpha 9$) linked by a long loop (residues 185-200) to Domain II. The substrate-binding site of the main protease is positioned at a cleft between domains I and II [55].

Molecular docking studies of FDA-approved anticancer drugs, Capmatinib, Pemigatinib, Selpercatinib, and Tucatinib, with the SARS-CoV-2 main protease, were achieved individually. From Figure 5, it can be inferred that the selected anticancer drugs (blue sticks) were capable of binding to SARS-CoV-2 main protease with binding energies (ΔG) of -8.0, -6.7, -7.4, and -7.8 kcal/mol, respectively. These binding energies provided an understanding of the binding affinity of the drug to the selected target. Usually, a low docking score is indicative of a more potent inhibition. The binding affinity of anticancer drugs was in the order Capmatinib > Tucatinib > Selpercatinib > Pemigatinib. The docking analysis of anticancer drugs within the active binding sites of SARS-CoV-2 main protease (PDB ID: 6LU7) are displayed in Table 4 and Figure 6. Analysis of docked poses of investigated drugs suggested that they exhibited several hydrophobic and some hydrophilic interactions with main residues of the interface. The stability of the enzyme-inhibitor complex is governed by hydrogen bonding [56].

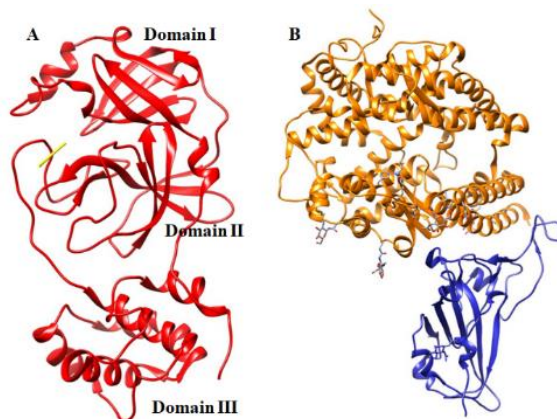
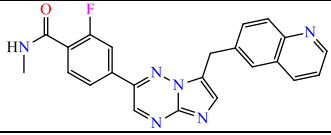
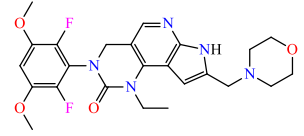
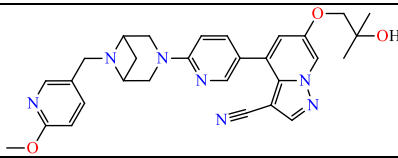
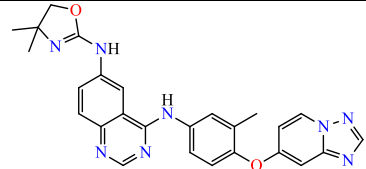


Figure 4. Model of the (A) SARS-CoV-2 main protease (PDB ID: 6LU7) and (B) SARS-CoV-2 spike glycoprotein (PDB ID: 6M0J) generated using CHIMERA [37].

Table 4 sums up the amino acid residues of the target sites that are involved in the hydrogen bonding with the selected anticancer drugs. The total binding strength is due to various types of bonds that include ionic, hydrophobic, and Vander Waals interactions; however, hydrogen bonding is a major contributor [57,58].

Table 4. Binding energies (kcal/mol) and amino acid residues involved in hydrogen bonding of investigated anticancer drugs within the binding sites of SARS-CoV-2 main protease (PDB ID:6LU7) and SARS-CoV-2 spike glycoprotein (PDB ID:6M0J).

Drug {Drug Bank Number}	Chemical structure	Targets	Receptor residues involved in Hydrogen bonding	Binding energy (kcal/mol)
Capmatinib 1 {DB11791}		6LU7	GlnA:110, LysA:102	-8.0
		6M0J	TyrA:196	-9.3
Pemigatinib 2 {DB15102}		6LU7	PheA:294	-6.7
		6M0J	ArgA:514, GlnA:98, LysA:562	-8.1
Selpercatinib 3 {DB15685}		6LU7	AspA:245, ThrA:243	-7.4
		6M0J	ArgA:514, AspA:350, GlnA:398	-8.7
Tucatinib 4 {DB11652 (DB06142)}		6LU7	-	-7.8
		6M0J	AspA:350, SerA:44	-9.6

A: Chain A of target enzyme; Arg-arginine; Asp-Asparagine; Gln-Glutamine; Lys-Lysine; Phe-phenylalanine; Thr-Threonine; Tyr-Tyrosine; Ser-serine.

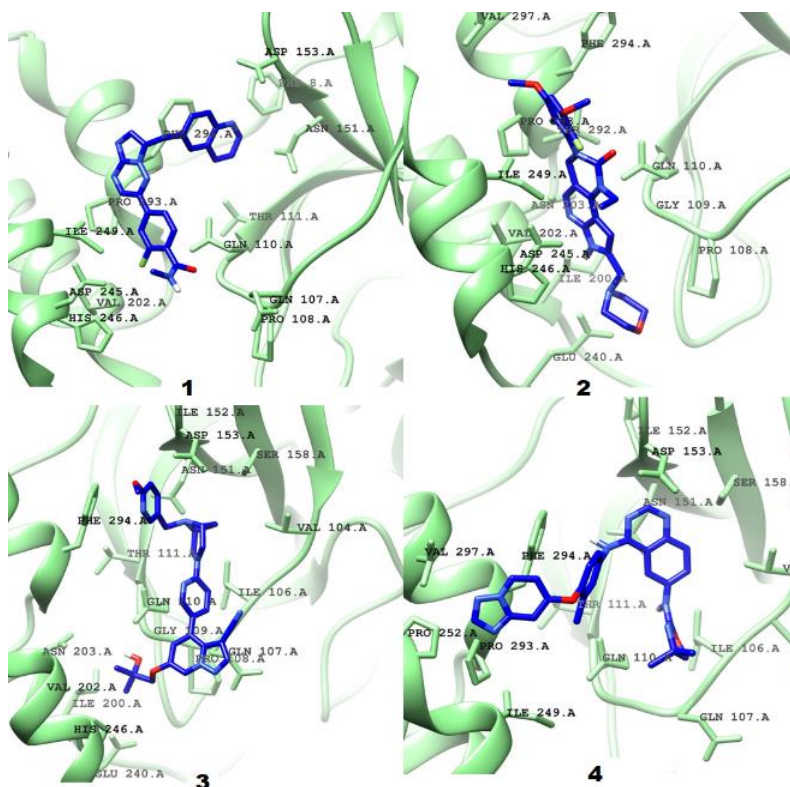


Figure 5. Molecular docking interactions of Capmatinib (1), Pemigatinib (2), Selpercatinib (3), and Tucatinib (4) displaying amino acid residues with SARS-CoV-2 main protease (PDB ID: 6LU7).

Hydrogen bonding is believed to depend on the composition and 3D alignment of contacting amino acid residues at the prominent and active binding sites [59]. The predicted active site amino acid residues of SARS-CoV-2 main protease (PDB ID: 6LU7) with Capmatinib are GlnA:110, LysA:102, PheA:294, ValA:104, IleA:106, ThrA:111, and AsnA:151. Among these, GlnA:110 and LysA:102 form hydrogen bonding with the drug Capmatinib, while other interactions such as π - π stacking (PheA:294), Vander Waal's forces (ValA:104, IleA:106, ThrA:111), and π -donor hydrogen bond with AsnA:151. Table 5 shows the various types of interactions apart from hydrogen bonding that is involved in the binding of Capmatinib, Pemigatinib, Selpercatinib, and Tucatinib with SARS-CoV-2 main protease (PDB ID: 6LU7).

Table 5. Type of interactions involved with the residues of the targets.

SARS-COV-2 main protease (6LU7)					
Type of Interactions	Amino acid residues				
	Capmatinib	Pemigatinib	Selpercatinib	Tucatinib	
Hydrogen bond	GlnA:110, LysA:102	PheA:294	AspA:245, ThrA:243	-	
π - π stacking	PheA:294	-	HisA:246, PheA:294	-	
Vander Waal's forces	IleA:106, ThrA:111, ValA:104	AspA:245, AsnA:203, GlnA:110, GlyA:109, HisA:246, IleA:200, ThrA:292	AsnA:203, GlnA:110, GluA:240, GlyA:109, IleA:200, ProA:108, ThrA:292	ArgA:105, AsnA:151, GlnA:107, HisA:246, IleA:106, PheA:294, ThrA:292	
π -alkyl	-	ProA:293, ValA:202,297	ProA:293, ValA:202	IleA:249, ValA:202	
Other	AsnA:151 (π -donor hydrogen bond)	IleA:249 (π - σ)	IleA:249 (π - σ)	-	
SARS-COV-2 spike glycoprotein (6M0J)					
Type of Interactions	Amino acid residues				
	Capmatinib	Pemigatinib	Selpercatinib	Tucatinib	
Hydrogen bond	TyrA:196	ArgA:514, GlnA:98, LysA:562	ArgA:514, AspA:350, GlnA:398	AspA:350, SerA:44	
π - π stacking	GlyA:205	-	HisA:401	PheA:40, TrpA:349	
Vander Waal's forces	AlaA:396, GluA:208, 398,564, GlyA:98,102, ProA:265, TrpA:203	AspA:200, GlnA:102, GluA:398, LeuA:392, TyrA:510	AspA:382, AsnA:397, HisA:378, LeuA:392, TrpA:349, TyrA:385	AlaA:348, ArgA:393, LeuA:351, LysA:562, SerA:43, TrpA:69	
π -alkyl	ValA:209	AlaA:99, LeuA:95	PheA:40,390	-	
Other	LysA:562 (π - cation) TyrA:202 (Fluorine)	-	-	-	

A: Chain A of target enzyme; Ala: alanine; Arg: arginine; Asn: asparagine; Asp: aspartate; Gln: glutamine; Glu: glutamate; Gly: glycine; His: histidine; Ile: isoleucine; Leu: leucine; Lys: lysine; Phe: phenylalanine; Pro: proline; Ser: serine; Thr: threonine; Trp: tryptophan; Tyr: tyrosine.

These results of docking analysis revealed that all the selected drugs except Tucatinib were capable of forming hydrogen bonds with amino acid residues in the active sites. From the above findings, we concluded that the differences because of the presence of interacting amino acids sharing active binding sites, with small association with or without hydrogen bonding. We also concluded that the presence of the hydrogen bonding was independent, with the regularity of interacting amino acids to active binding sites and docking strength.

3.3.2. Docking with SARS-CoV-2 spike glycoprotein.

The coronavirus spike glycoprotein comprises of three cleavage sites that are administered by human host proteases (Figure 4B). The level of viral pathogenicity and cross-species can be determined only by understanding the exact nature of cleavage sites and their individual processing proteases. The outer surface of coronaviruses (including SARS-CoV-2) holds a critical transmembrane spike glycoprotein that is necessary for their entry into the host cells. This viral glycoprotein possesses a crown-like trimeric structure, containing domains and structural motifs essential for binding to host cells and for viral replication. In this context, two

The results revealed their good binding with SARS-CoV-2 spike glycoprotein with ΔG values in the order Tucatinib (-9.6 kcal/mol) > Capmatinib (-9.3 kcal/mol) > Selpercatinib (-8.7 kcal/mol) > Pemigatinib (-8.1 kcal/mol). Tables 4 and 5 lists the amino acid residues involved in the binding of the drugs with SARS-CoV-2 spike glycoprotein (PDB ID: 6M0J) and the types of interactions inferred. Figure 9 displays the histogram representing the binding energies, ΔG (kcal/mol) of investigated drugs with the targets.

These findings of the molecular docking results were found to be in agreeable corroboration with the results of DFT calculations, proposing Capmatinib as the potent drug that could be used for the treatment of COVID-19, since it was found to bind with both the targets and also exhibited strong intermolecular interactions. Further, these selected FDA-approved anticancer drugs were capable of binding to the new coronavirus strain SARS-CoV-2 main protease and SARS-CoV-2 spike glycoprotein firmly and, as a result, could probably inhibit the functioning of the polymerase.

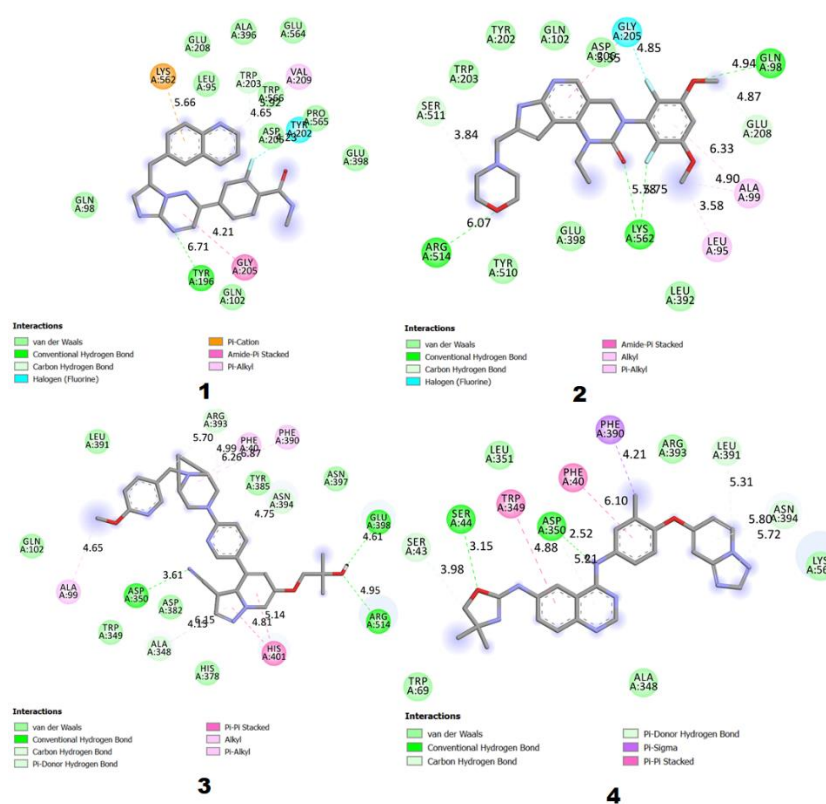


Figure 8. 2D interaction profile of Capmatinib (1), Pemigatinib (2), Selpercatinib (3), and Tucatinib (4) with SARS-CoV-2 spike glycoprotein.

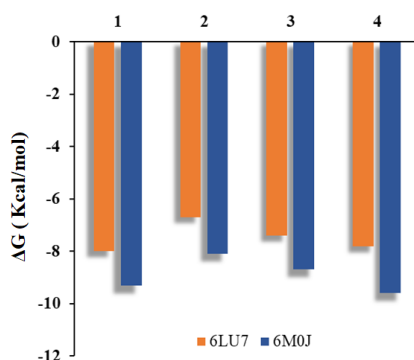


Figure 9. Histogram representing the binding energies, ΔG (kcal/mol) of Capmatinib (1), Pemigatinib (2), Selpercatinib (3), and Tucatinib (4).

4. Conclusions

To combat the lethal coronavirus contagion, several studies are being carried out utilizing anticancer drug treatments. In this paper, we report four recent FDA-approved anticancer drugs, Capmatinib, Pemigatinib, Selpercatinib, and Tucatinib, that have been investigated for their potential use for against SARS-CoV-2 *via* molecular docking and DFT calculations. The ADME properties and drug-likeness suggested their good oral bioavailability. DFT exploration of the selected drugs also displayed acceptable results. Molecular docking calculations were achieved to evaluate the binding interaction of the investigated anticancer drugs with the SARS-CoV-2 targets (i) SARS-CoV-2 main protease (PDB ID: 6LU7), and (ii) SARS-CoV-2 spike glycoprotein (PDB ID: 6M0J). The results of which revealed multiple hydrogen-bonding interactions, with the active amino acid residues with the binding energies of -8.0, -6.7, -7.4, and -7.8 kcal/mol for Capmatinib, Pemigatinib, Selpercatinib, and Tucatinib, respectively with SARS-CoV-2 main protease (6LU7). On the other hand, the calculated ΔG values were -9.3, -8.1, -8.7, and -9.6 kcal/mol respectively for Capmatinib, Pemigatinib, Selpercatinib, and Tucatinib, with SARS-CoV-2 spike glycoprotein (6M0J). Thus, these anticancer drugs, *viz.*, Capmatinib, Pemigatinib, Selpercatinib, and Tucatinib, could be investigated *via* experimental findings in the future clinical trials of drugs against SARS-CoV-2. We also hope that our preliminary findings could provide a path for a more comprehensive clinical investigation on the repurposing strategy of previously existing anticancer drugs for treating COVID-19, a track of research sustained by limited funds but of principal significance to face this new worldwide challenge.

Funding

This research received no external funding.

Acknowledgments

The author is grateful to Taibah University.

Conflicts of Interest

The authors declare no conflict of interest.

References

1. <https://www.who.int/dg>.
2. Benvenuto, D.; Giovanetti, M.; Salemi, M.; Prosperi, M.; De Flora, C.; Junior Alcantara, L.C.; Angeletti, S.; Ciccozzi, M. The global spread of 2019-nCoV: a molecular evolutionary analysis. *Pathog. Glob. Health* **2020**, *114*, 64–67, <https://doi.org/10.1080/20477724.2020.1725339>.
3. Channappanavar, R.; Perlman, S. Pathogenic human coronavirus infections: causes and consequences of cytokine storm and immunopathology. *Semin. Immunopathol.* **2017**, *39*, 529–539, <https://doi.org/10.1007/s00281-017-0629-x>.
4. Ji, W.; Wang, W.; Zhao, X.; Zai, J.; Li, X. Cross-species transmission of the newly identified coronavirus 2019-nCoV. *J. Med. Virol.* **2020**, <https://doi.org/10.1002/jmv.25682>.
5. Ibrahim, I.M.; Abdelmalek, D.H.; Elshahat, M.E.; Elfiky, A.A. COVID-19 spike-host cell receptor GRP78 binding site prediction. *J. Infect.* **2020**, *80*, 554–562, <https://doi.org/10.1016/j.jinf.2020.02.026>.
6. Ibrahim, I.M.; Abdelmalek, D.H.; Elfiky, A.A. GRP78: A cell's response to stress. *Life Sci.* **2019**, *226*, 156–163, <https://doi.org/10.1016/j.lfs.2019.04.022>.
7. Khalid, Z.; Naveed, H. Identification of destabilizing SNPs in SARS-CoV2-ACE2 protein and spike glycoprotein: implications for virus entry mechanisms. *J. Biomol. Struct. Dyn.* **2020**, 1–11, <https://doi.org/10.1080/07391102.2020.1823885>.

8. Parvathaneni, V.; Kulkarni, N.S.; Muth, A.; Gupta, V. Drug repurposing: a promising tool to accelerate the drug discovery process. *Drug Discov. Today* **2019**, *24*, 2076–2085, <https://doi.org/10.1016/j.drudis.2019.06.014>.
9. Naylor, S.; Kauppi, D.M.; Schonfeld, J.M. Therapeutic drug repurposing, repositioning and rescue: Part II: Business review. *Drug Discov. World* **2015**, *16*, 57–72.
10. Rameshrad, M.; Ghafoori, M.; Mohammadpour, A.H.; Nayeri, M.J.D.; Hosseinzadeh, H. A comprehensive review on drug repositioning against coronavirus disease 2019 (COVID19). *Naunyn. Schmiedebergs. Arch. Pharmacol.* **2020**, *393*, 1137–1152, <https://doi.org/10.1007/s00210-020-01901-6>.
11. Rothan, H.A.; Byrareddy, S.N. The epidemiology and pathogenesis of coronavirus disease (COVID-19) outbreak. *J. Autoimmun.* **2020**, *109*, <https://doi.org/10.1016/j.jaut.2020.102433>.
12. Liu, C.; Zhou, Q.; Li, Y.; Garner, L. V.; Watkins, S.P.; Carter, L.J.; Smoot, J.; Gregg, A.C.; Daniels, A.D.; Jervey, S.; Albau, D. Research and Development on Therapeutic Agents and Vaccines for COVID-19 and Related Human Coronavirus Diseases. *ACS Cent. Sci.* **2020**, *6*, 315–331, <https://doi.org/10.1021/acscentsci.0c00272>.
13. Linton, N.M.; Kobayashi, T.; Yang, Y.; Hayashi, K.; Akhmetzhanov, A.R.; Jung, S.; Yuan, B.; Kinoshita, R.; Nishiura, H. Incubation Period and Other Epidemiological Characteristics of 2019 Novel Coronavirus Infections with Right Truncation: A Statistical Analysis of Publicly Available Case Data. *J. Clin. Med.* **2020**, *9*, <https://doi.org/10.3390/jcm9020538>.
14. Ciliberto, G.; Mancini, R.; Paggi, M.G. Drug repurposing against COVID-19: focus on anticancer agents. *J. Exp. Clin. Cancer Res.* **2020**, *39*, <https://doi.org/10.1186/s13046-020-01590-2>.
15. Wahedi, H.M.; Ahmad, S.; Abbasi, S.W. Stilbene-based natural compounds as promising drug candidates against COVID-19. *J. Biomol. Struct. Dyn.* **2020**, 1–10, <https://doi.org/10.1080/07391102.2020.1762743>.
16. Kumar, A.; Choudhir, G.; Shukla, S.K.; Sharma, M.; Tyagi, P.; Bhushan, A.; Rathore, M. Identification of phytochemical inhibitors against main protease of COVID-19 using molecular modeling approaches. *J. Biomol. Struct. Dyn.* **2020**, 1–11, <https://doi.org/10.1080/07391102.2020.1772112>.
17. Iftikhar, H.; Ali, H.N.; Farooq, S.; Naveed, H.; Shahzad-ul-Hussan, S. Identification of potential inhibitors of three key enzymes of SARS-CoV2 using computational approach. *Comput. Biol. Med.* **2020**, *122*, <https://doi.org/10.1016/j.compbimed.2020.103848>.
18. Owis, A.I.; El-Hawary, M.S.; El Amir, D.; Aly, O.M.; Abdelmohsen, U.R.; Kamel, M.S. Molecular docking reveals the potential of *Salvadora persica* flavonoids to inhibit COVID-19 virus main protease. *RSC Adv.* **2020**, *10*, 19570–19575, <https://doi.org/10.1039/D0RA03582C>.
19. Santibáñez-Morán, M.G.; López-López, E.; Prieto-Martínez, F.D.; Sánchez-Cruz, N.; Medina-Franco, J.L. Consensus virtual screening of dark chemical matter and food chemicals uncover potential inhibitors of SARS-CoV-2 main protease. *RSC Adv.* **2020**, *10*, 25089–25099, <https://doi.org/10.1039/D0RA04922K>.
20. Sang, P.; Tian, S.-H.; Meng, Z.-H.; Yang, L.-Q. Anti-HIV drug repurposing against SARS-CoV-2. *RSC Adv.* **2020**, *27*, 15775–15783, <https://doi.org/10.1039/D0RA01899F>.
21. Sharma, P.; Shanavas, A. Natural derivatives with dual binding potential against SARS-CoV-2 main protease and human ACE2 possess low oral bioavailability: a brief computational analysis. *J. Biomol. Struct. Dyn.* **2020**, 1–12, <https://doi.org/10.1080/07391102.2020.1794970>.
22. Mittal, L.; Kumari, A.; Srivastava, M.; Singh, M.; Asthana, S. Identification of potential molecules against COVID-19 main protease through structure-guided virtual screening approach. *J. Biomol. Struct. Dyn.* **2020**, 1–19, <https://doi.org/10.1080/07391102.2020.1768151>.
23. Barile, E.; Baggio, C.; Gambini, L.; Shiryayev, S.A.; Strongin, A.Y.; Pellicchia, M. Potential Therapeutic Targeting of Coronavirus Spike Glycoprotein Priming. *Molecules* **2020**, *25*, <https://doi.org/10.3390/molecules25102424>.
24. Musarrat, F.; Chouljenko, V.; Dahal, A.; Nabi, R.; Chouljenko, T.; Jois, S.D.; Kousoulas, K.G. The anti-HIV drug nelfinavir mesylate (Viracept) is a potent inhibitor of cell fusion caused by the SARS-CoV-2 spike (S) glycoprotein warranting further evaluation as an antiviral against COVID-19 infections. *J. Med. Virol.* **2020**, *92*, 2087–2095, <https://doi.org/10.1002/jmv.25985>.
25. Sehailia, M.; Chemat, S. Antimalarial-agent artemisinin and derivatives portray more potent binding to Lys353 and Lys31-binding hotspots of SARS-CoV-2 spike protein than hydroxychloroquine: potential repurposing of arteminol for COVID-19. *J. Biomol. Struct. Dyn.* **2020**, 1–11, <https://doi.org/10.1080/07391102.2020.1796809>.
26. Bacha, U.; Barrila, J.; Velazquez-Campoy, A.; Leavitt, S.A.; Freire, E. Identification of Novel Inhibitors of the SARS Coronavirus Main Protease 3CL pro[†]. *Biochemistry* **2004**, *43*, 4906–4912, <https://doi.org/10.1021/bi0361766>.
27. Daina, A.; Michielin, O.; Zoete, V. SwissTargetPrediction: updated data and new features for efficient prediction of protein targets of small molecules. *Nucleic Acids Res.* **2019**, *47*, W357–W364.
28. Schmidt, M.W.; Baldrige, K.K.; Boatz, J.A.; Elbert, S.T.; Gordon, M.S.; Jensen, J.H.; Koseki, S.; Matsunaga, N.; Nguyen, K.A.; Su, S.; Windus, T.L.; Dupuis, M.; Montgomery, Jr. J.A. General atomic and molecular electronic structure system. *J. Comput. Chem.* **1993**, *14*, 1347–1363, <https://doi.org/10.1002/jcc.540141112>.
29. Gordon, M.S.; Schmidt, M.W. Advances in electronic structure theory. In: *Theory and Applications of*

- Computational Chemistry*. Elsevier, **2005**; pp. 1167–1189.
30. Shahab, S.; Sheikhi, M.; Filippovich, L.; Anatol'evich, D.E.; Yahyaei, H. Quantum chemical modeling of new derivatives of (E,E)-azomethines: Synthesis, spectroscopic (FT-IR, UV/Vis, polarization) and thermophysical investigations. *J. Mol. Struct.* **2017**, *1137*, 335–348, <https://doi.org/10.1016/j.molstruc.2017.02.056>.
 31. Shahab, S.; Filippovich, L.; Sheikhi, M.; Kumar, R.; Dikumar, E.; Yahyaei, H.; Muravsky, A. Polarization, excited states, trans-cis properties and anisotropy of thermal and electrical conductivity of the 4-(phenyldiazenyl)aniline in PVA matrix. *J. Mol. Struct.* **2017**, *1141*, 703–709, <https://doi.org/10.1016/j.molstruc.2017.04.014>.
 32. Shahab, S. Spectroscopic (Polarization, ExcitedState, FT-IR, UV/Vis and ¹H NMR) and Thermophysical Investigations of New Synthesized Azo Dye and Its Application in Polarizing Film. *Am. J. Mater. Synth. Process.* **2017**, *2*, 17, <https://doi.org/10.11648/j.ajmsp.20170202.11>.
 33. Trott, O.; Olson, A.J. AutoDock Vina: Improving the speed and accuracy of docking with a new scoring function, efficient optimization, and multithreading. *J. Comput. Chem.* **2009**, *31*, 455–461, <https://doi.org/10.1002/jcc.21334>.
 34. Jin, Z.; Du, X.; Xu, Y.; Deng, Y.; Liu, M.; Zhao, Y.; Zhang, B.; Li, X.; Zhang, L.; Peng, C.; Duan, Y.; Yu, J.; Wang, L.; Yang, K.; Liu, F.; Jiang, R.; Yang, X.; You, T.; Liu, X.; Yang, X.; Bai, F.; Liu, H.; Liu, X.; Guddat, L.W.; Xu, W.; Xiao, G.; Qin, C.; Shi, Z.; Jiang, H.; Rao, Z.; Yang, H. Structure of Mpro from SARS-CoV-2 and discovery of its inhibitors. *Nature* **2020**, *582*, 289–293, <https://doi.org/10.1038/s41586-020-2223-y>.
 35. Kirchdoerfer, R.N.; Ward, A.B. Structure of the SARS-CoV nsp12 polymerase bound to nsp7 and nsp8 cofactors. *Nat. Commun.* **2019**, *10*, <https://doi.org/10.1038/s41467-019-10280-3>.
 36. Morris, G.M.; Huey, R.; Lindstrom, W.; Sanner, M.F.; Belew, R.K.; Goodsell, D.S.; Olson, A.J. AutoDock4 and AutoDockTools4: Automated docking with selective receptor flexibility. *J. Comput. Chem.* **2009**, *30*, 2785–2791, <https://doi.org/10.1002/jcc.21256>.
 37. Pettersen, E.F.; Goddard, T.D.; Huang, C.C.; Couch, G.S.; Greenblatt, D.M.; Meng, E.C.; Ferrin, T.E. UCSF Chimera?A visualization system for exploratory research and analysis. *J. Comput. Chem.* **2004**, *25*, 1605–1612, <https://doi.org/10.1002/jcc.20084>.
 38. BIOVIA, Dassault Systèmes, Discovery studio visualizer, 2020, San Diego: D.S. **2020**.
 39. Cheng, W.; Yuan, Y.; Qiu, N.; Peng, P.; Sheng, R.; Hu, Y. Identification of novel 4-anilinoquinazoline derivatives as potent EGFR inhibitors both under normoxia and hypoxia. *Bioorganic Med. Chem.* **2014**, *22*, 6796–6805, <https://doi.org/10.1016/j.bmc.2014.10.038>.
 40. Lipinski, C.A.; Lombardo, F.; Dominy, B.W.; Feeney, P.J. Experimental and computational approaches to estimate solubility and permeability in drug discovery and development settings. *Adv. Drug Deliv. Rev.* **1997**, *23*, 3–25, [https://doi.org/10.1016/S0169-409X\(96\)00423-1](https://doi.org/10.1016/S0169-409X(96)00423-1).
 41. Abdel-Mohsen, H.T.; Abood, A.; Flanagan, K.J.; Meindl, A.; Senge, M.O.; El Diwani, H.I. Synthesis, crystal structure, and ADME prediction studies of novel imidazopyrimidines as antibacterial and cytotoxic agents. *Arch. Pharm. (Weinheim)*. **2020**, *353*, <https://doi.org/10.1002/ardp.201900271>.
 42. Pliška, V.; Testa, B.; van de Waterbeemd, H. *Lipophilicity in Drug Action and Toxicology*. Volume 4, **2008**; <https://doi.org/10.1002/9783527614998>.
 43. Arnott, J.A.; Planey, S.L. The influence of lipophilicity in drug discovery and design. *Expert Opin. Drug Discov.* **2012**, *7*, 863–75, <https://doi.org/10.1517/17460441.2012.714363>.
 44. Ottaviani, G.; Gosling, D.J.; Patissier, C.; Rodde, S.; Zhou, L.; Faller, B. What is modulating solubility in simulated intestinal fluids? *Eur. J. Pharm. Sci.* **2010**, *41*, 452–457, <https://doi.org/10.1016/j.ejps.2010.07.012>.
 45. Savjani, K.T.; Gajjar, A.K.; Savjani, J.K. Drug Solubility: Importance and Enhancement Techniques. *ISRN Pharm.* **2012**, *2012*, 1–10, <https://doi.org/10.5402/2012/195727>.
 46. Daina, A.; Michielin, O.; Zoete, V. SwissADME: A free web tool to evaluate pharmacokinetics, drug-likeness and medicinal chemistry friendliness of small molecules. *Sci. Rep.* **2017**, *7*, <https://doi.org/10.1038/srep42717>.
 47. Zheng, Y.; Zheng, M.; Ling, X.; Liu, Y.; Xue, Y.; An, L.; Gu, N.; Jin, M. Design, synthesis, quantum chemical studies and biological activity evaluation of pyrazole–benzimidazole derivatives as potent Aurora A/B kinase inhibitors. *Bioorg. Med. Chem. Lett.* **2013**, *23*, 3523–3530, <https://doi.org/10.1016/j.bmcl.2013.04.039>.
 48. Middleton, E.; Kandaswami, C.; Theoharides, T.C. The effects of plant flavonoids on mammalian cells: implications for inflammation, heart disease, and cancer. *Pharmacol. Rev.* **2000**, *52*, 673–751.
 49. Xavier, S.; Periandy, S.; Ramalingam, S. NBO, conformational, NLO, HOMO–LUMO, NMR and electronic spectral study on 1-phenyl-1-propanol by quantum computational methods. *Spectrochim. Acta Part A Mol. Biomol. Spectrosc.* **2015**, *137*, 306–320, <https://doi.org/10.1016/j.saa.2014.08.039>.
 50. da Silva, J.K.R.; Figueiredo, P.L.B.; Byler, K.G.; Setzer, W.N. Essential Oils as Antiviral Agents, Potential of Essential Oils to Treat SARS-CoV-2 Infection: An In-Silico Investigation. *Int. J. Mol. Sci.* **2020**, *21*, <https://doi.org/10.3390/ijms21103426>.
 51. Bzówka, M.; Mitusińska, K.; Raczyńska, A.; Samol, A.; Tuszyński, J.A.; Góra, A. Structural and

- Evolutionary Analysis Indicate That the SARS-CoV-2 Mpro Is a Challenging Target for Small-Molecule Inhibitor Design. *Int. J. Mol. Sci.* **2020**, *21*, <https://doi.org/10.3390/ijms21093099>.
52. Gimeno, A.; Mestres-Truyol, J.; Ojeda-Montes, M.J.; Macip, G.; Saldivar-Espinoza, B.; Cereto-Massagué, A.; Pujadas, G.; Garcia-Vallvé, S. Prediction of Novel Inhibitors of the Main Protease (M-pro) of SARS-CoV-2 through Consensus Docking and Drug Reposition. *Int. J. Mol. Sci.* **2020**, *21*, <https://doi.org/10.3390/ijms21113793>.
 53. Kojetin, D.J.; Burris, T.P. Small Molecule Modulation of Nuclear Receptor Conformational Dynamics: Implications for Function and Drug Discovery. *Mol. Pharmacol.* **2013**, *83*, 1–8, <https://doi.org/10.1124/mol.112.079285>.
 54. Schena, A.; Griss, R.; Johnsson, K. Modulating protein activity using tethered ligands with mutually exclusive binding sites. *Nat. Commun.* **2015**, *6*, <https://doi.org/10.1038/ncomms8830>.
 55. Zhang, L.; Lin, D.; Sun, X.; Curth, U.; Drosten, C.; Sauerhering, L.; Becker, S.; Rox, K.; Hilgenfeld, R. Crystal structure of SARS-CoV-2 main protease provides a basis for design of improved a-ketoamide inhibitors. *Science (80-.)* **2020**, *368*, 409–412, <https://doi.org/10.1126/science.abb3405>.
 56. Du, X.; Li, Y.; Xia, Y.-L.; Ai, S.-M.; Liang, J.; Sang, P.; Ji, X.-L.; Liu, S.-Q. Insights into Protein–Ligand Interactions: Mechanisms, Models, and Methods. *Int. J. Mol. Sci.* **2016**, *17*, 144, <https://doi.org/10.3390/ijms17020144>.
 57. Papanephytous, C.P.; Grigoroudis, A.I.; McInnes, C.; Kontopidis, G. Quantification of the Effects of Ionic Strength, Viscosity, and Hydrophobicity on Protein–Ligand Binding Affinity. *ACS Med. Chem. Lett.* **2014**, *5*, 931–936, <https://doi.org/10.1021/ml500204e>.
 58. Zhao, X.; Xu, Z.; Li, H. NSAIDs Use and Reduced Metastasis in Cancer Patients: results from a meta-analysis. *Sci. Rep.* **2017**, *7*, <https://doi.org/10.1038/s41598-017-01644-0>.
 59. Chelliah, V.; Blundell, T.L.; Fernández-Recio, J. Efficient Restraints for Protein–Protein Docking by Comparison of Observed Amino Acid Substitution Patterns with those Predicted from Local Environment. *J. Mol. Biol.* **2006**, *357*, 1669–1682, <https://doi.org/10.1016/j.jmb.2006.01.001>.
 60. Wrapp, D.; Wang, N.; Corbett, K.S.; Goldsmith, J.A.; Hsieh, C.L.; Abiona, O.; Graham, B.S.; McLellan, J.S. Cryo-EM structure of the 2019-nCoV spike in the prefusion conformation. *Science (80-.)*. **2020**, <https://doi.org/10.1126/science.abb2507>.
 61. Coutard, B.; Valle, C.; de Lamballerie, X.; Canard, B.; Seidah, N.G.; Decroly, E. The spike glycoprotein of the new coronavirus 2019-nCoV contains a furin-like cleavage site absent in CoV of the same clade. *Antiviral Res.* **2020**, *176*, <https://doi.org/10.1016/j.antiviral.2020.104742>.
 62. Hoffmann, M.; Kleine-Weber, H.; Schroeder, S.; Krüger, N.; Herrler, T.; Erichsen, S.; Schiergens, T.S.; Herrler, G.; Wu, N.H.; Nitsche, A.; Müller, M.A.; Drosten, C.; SARS-CoV-2 Cell Entry Depends on ACE2 and TMPRSS2 and Is Blocked by a Clinically Proven Protease Inhibitor. *Cell* **2020**, *181*, 271–280, <https://doi.org/10.1016/j.cell.2020.02.052>.

*<https://www.fda.gov/drugs/drug-approvals-and-databases/fda-grants-accelerated-approval-Capmatinib-metastatic-non-small-cell-lung-cancer>

†<https://www.fda.gov/drugs/resources-information-approved-drugs/fda-grants-accelerated-approval-Pemigatinib-cholangiocarcinoma-fgfr2-rearrangement-or-fusion>

‡<https://www.fda.gov/drugs/drug-approvals-and-databases/fda-approves-Selpercatinib-lung-and-thyroid-cancers-ret-gene-mutations-or-fusions>

‡‡<https://www.fda.gov/drugs/resources-information-approved-drugs/fda-approves-Tucatinib-patients-her2-positive-metastatic-breast-cancer>